International Journal of Fracture **95:** 67–88, 1999.

Scale effects in the initiation of cracking of a scarf joint

D. LIU and N.A. FLECK
Cambridge University, Engineering Department, Trumpington Street, Cambridge, CB2 1PZ, U.K. e-mail: naf1@eng.cam.ac.uk

Received 23 July 1998; accepted in revised form 31 December 1998

Abstract. The singular stress field at the interface-corner of a bi-material scarf joint is analysed for a strip of finite width, w, under remote tension and bending. The two substrates are taken as linear elastic and isotopic. The intensity of the singular stress field is calculated using a domain integral method, and is plotted as a function of joint geometry and material mismatch parameters. It is envisaged that the intensity of singularity can serve as a valid fracture criterion provided the zone of nonlinearity is fully embedded within the singular elastic field. It is assumed that fracture initiates when the magnitude of the corner singularity attains a critical value; consequently, the fracture strength of the joint depends upon the size of the structure. In addition, the interfacial stress intensity factor and the associated T-stress are determined for an edge interfacial crack. When the crack is short with respect to the width of the strip, the stress intensity factor is dominated by the presence of the corner singularity; a boundary layer formulation is used to determine the coupling between the crack tip field and the interface-corner field. The solution suggests that an interfacial crack grows unstably with a rapidly increasing energy release rate, but with only a small change in mode mix.

Key words: Scale effects, size effects, interfacial fracture, initiation of failure, scarf joint, domain integral, corner singularity.

1. Introduction

Adhesive bonding of dissimilar parts is increasingly used in the aerospace, automotive and electronic industries as this technology offers a number of attractive features, including high strength to weight ratio, improved appearance, improved corrosion resistance and cost effectiveness (Kinloch, 1987). Scarf joints are preferable to butt joints as the adhesive is loaded by a combination of shear and tension rather than in a tensile peel mode, giving higher joint strengths. The failure of bonded joints often initiates at the corner singularity where the interface intersects a traction-free edge. Therefore, the analysis of the singular stress field at an interface-corner is fundamental to an understanding of the initiation of failure from the free-edge of a joint.

Consider the problem of two wedges of apex angles θ_1 and θ_2, made from linear elastic and isotropic solids, 1 and 2, respectively, as sketched in Figure 1. A stress singularity of algebraic type $Hr^{\lambda-1}$ exists at the interface-corner for λ less than unity. Here, r is the radial distance from the corner, H is the intensity of the singularity and the order of the stress singularity, $\lambda - 1$, may be real or complex. The H-singularity occurs only within a local region near the interface-corner and is a free-edge effect (Akisanya and Fleck, 1997). An asymptotic analysis has been performed for an extensive range of material combinations and edge geometries, θ_1 and θ_2 (Bogy, 1971; Hein and Erdogan, 1971); the magnitude of λ depends upon the local wedge geometry and the mismatch in elastic parameters, but not upon the details of the overall geometry of the body. The intensity H characterises the amplitude of the singular stress field;

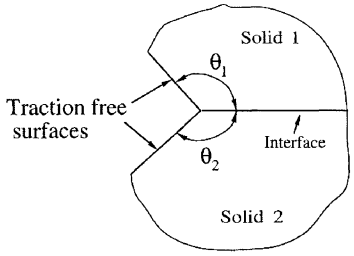

Figure 1. General configuration at the free-edge of two bonded dissimilar materials.

H scales linearly with the applied load on the body, and depends upon the degree of elastic mismatch, the overall geometry of the body, and upon the details of the loading on the body. A number of researchers (Gradin, 1982; Groth, 1988; Hattori et al., 1989) have proposed that H can be used as a crack initiation parameter, analogous to the crack tip stress intensity factor K for the onset of crack growth from a pre-existing crack. Failure is assumed to initiate at an interface-corner when the magnitude of H attains a critical value, H_c. The critical value H_c must be determined by experiments, or from a micromechanical model of the initiation of fracture. For example, we might envisage that the critical value H_c is associated with a normal stress component on the interface exceeding a critical value over a critical distance from the interface-corner.

Several experimental studies have validated the use of an H-based failure criterion for bi-material joints (Gradin, 1982; Groth, 1988; Hattori et al., 1989; Reedy and Guess, 1993; Qian and Akisanya, 1998). It is found that the critical value of the intensity H at crack initiation is insensitive to the global details of joint geometry, for a given wedge geometry and material combination. Finite element analysis has shown that the zone of material nonlinearity at failure is embedded within a region dominated by the H-field, and so the elastic parameter H_c is valid for the experimental systems considered (Reedy, 1993; Groth and Brottare, 1988). Since H is of dimension stress times length to the power $(1 - \lambda)$ the failure criterion $H = H_c$ implies that the remote failure stress scales with the leading dimension of the specimen to the power $(\lambda - 1)$. A specimen size effect is predicted such that the strength decreases with increasing specimen size. There is a growing body of evidence to support such a size effect (see for example, Reedy and Guess, 1993; Qian and Akisanya, 1998). Alternative sources of a size effect are the fractal nature of microcracking (Carpinteri, 1996), the statistics of pre-existing flaws (Weibull, 1939) and the dependence of the fracture process zone upon the structural size (Bazant, 1997).

Application of an H-based failure criterion requires detailed calibrations for the intensity H as a function of the joint overall geometry, material combinations and remote loading. Two methods have been used to extract the intensity H from finite element analysis:

(i) a comparison of the finite element solution for stress and displacement with the asymptotic field; and

(ii) a more accurate procedure, based on a contour integral method (Stern *et al.*, 1976; Sinclair et al., 1985; Carpenter and Byers, 1987).

The first method was used to determine H_c in most of the experimental studies mentioned above. This method has also been used in the theoretical analysis of free-edge singularities for mechanical and thermal loading; for example, Reedy (1990, 1993) considered a thin elastic layer sandwiched between two rigid substrates, and Munz and Yang (1992, 1993) examined

elastic bi-material wedges of various wedge angles. Akisanya and Fleck (1997) extended the second method to extract H by developing a domain integration method. They analysed the case of a butt joint between two long strips of dissimilar elastic solids. Using the same methodology, Qian and Akisanya (1997a, b) calculated the magnitude of the intensity H for a scarf joint between two long dissimilar strips, subjected to remote tension and thermal loading; they also considered a scarf joint comprising a thin sandwich layer between identical substrates. They found that a much denser mesh was needed to extract accurate values for H from the singular stress and displacement field (method 1) compared with the domain integral method (method 2).

1.1. LEVEL OF SINGULARITY IN A SCARF JOINT

In this study we shall address the scarf joint shown in the insert of Figure 2. The joint comprises two elastic strips made from dissimilar isotropic, elastic solids, and the bond line is inclined at an arbitrary inclination ω to the free surface. For the purposes of an asymptotic analysis of the stress state at the interface-corner, it may be assumed that the joint is subjected to arbitrary remote loading in equilibrium. For such a problem, Dundurs (1969) has shown that the stress distribution depends on only two combinations of the elastic constants. The two elastic mismatch parameters are defined by

$$\alpha = \frac{\mu_1(\kappa_2 + 1) - (\kappa_1 + 1)\mu_2}{\mu_1(\kappa_2 + 1) + (\kappa_1 + 1)\mu_2}, \tag{1a}$$

and

$$\beta = \frac{\mu_1(\kappa_2 - 1) - (\kappa_1 - 1)\mu_2}{\mu_1(\kappa_2 + 1) + (\kappa_1 + 1)\mu_2}, \tag{1b}$$

where the subscripts refer to materials 1 or 2. E_i and ν_i denote Young's modulus and Poisson's ratio for material i, respectively, the shear modulus is μ_i ($\equiv E_i/2(1+\nu_i)$) and $\kappa_i \equiv 3-4\nu_i$ for plane strain conditions. The (α, β) values for typical material combinations are concentrated between the $\beta = 0$ and $\beta = \alpha/4$ lines in $\alpha - \beta$ space (Suga et al., 1988). In the current paper, we restrict our attention to material combinations with $\beta = 0$ and $\beta = \alpha/4$, and we shall consider the bi-material body to be sufficiently thick for plane strain conditions to prevail.

Recall that the displacement field u_i at a distance r from the interface-corner of the scarf joint scales as Hr^{λ}, and the elastic stress and strain distributions scale as $Hr^{\lambda-1}$. The eigenvalue problem for λ has already been addressed by Qian and Akisanya (1997a), and the details are omitted here; the analysis follows that laid down by Stern et al. (1976) and by Carpenter and Byers (1987). Contours of λ for the interface-corner of a scarf joint are shown in Figure 2 as a function of the material mismatch parameter α and the interface inclination ω. Without loss of generality, we consider the range $0° \leqslant \omega \leqslant 90°$ and $|\alpha| \leqslant 1$. Results for λ are displayed for $\beta = 0$, and for $\beta = \alpha/4$. Recall that for $\lambda < 1$ the stresses are unbounded (singular) as the interface-corner is approached. For $\lambda \geqslant 1$ the stresses remain finite (nonsingular) at the interface-corner.

Consider first the case $\beta = 0$. The eigenvalue λ is real and the stresses are singular ($\lambda < 1$) or nonsingular ($\lambda \geqslant 1$) depending upon the particular choice of values for α and ω. For the special case $\alpha = 0$ the material mismatch vanishes and the asymptotic stress state consists of uniform tension parallel to the free surface, giving $\lambda = 1$. A solution comprising uniform

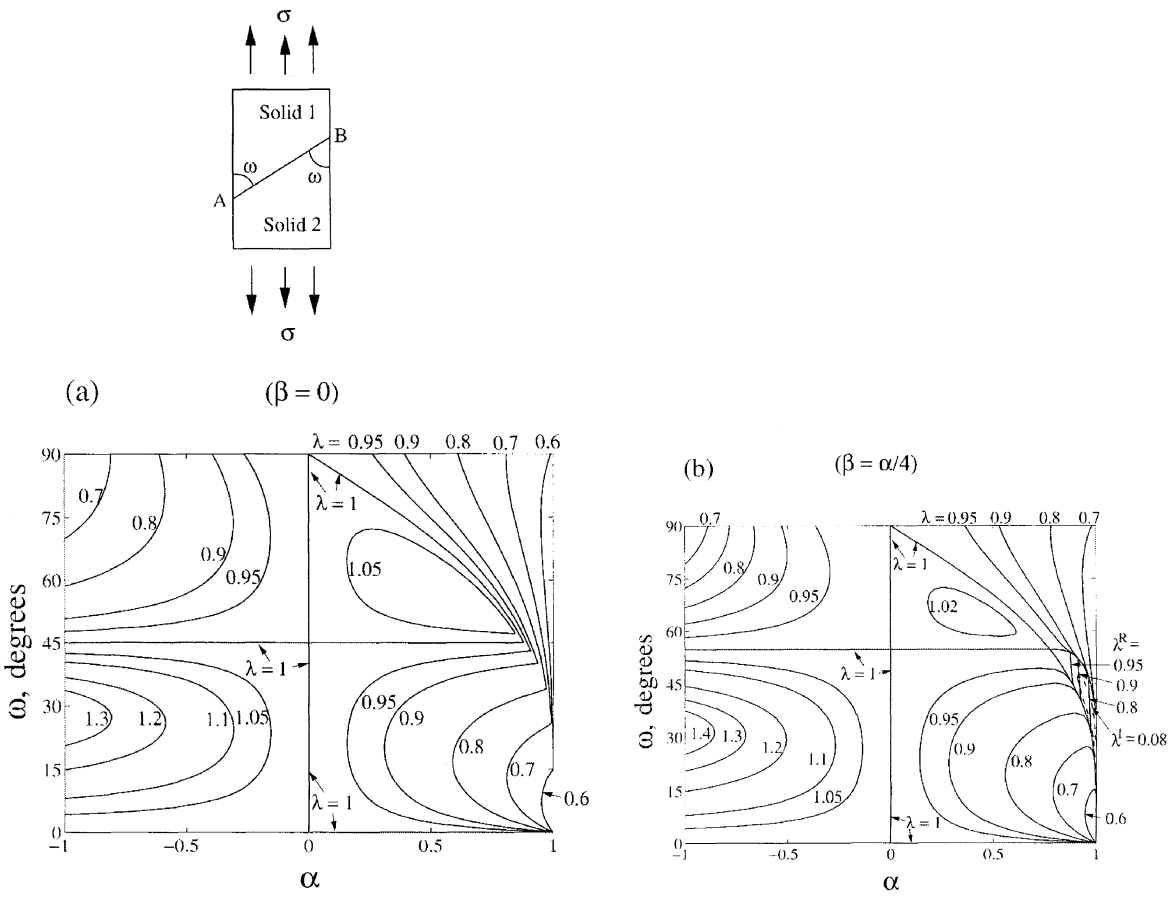

Figure 2. The level of displacement singularity λ at the interface-corner of a scarf joint, as a function of the material mismatch parameter α and the inclination ω of the interface. (a) $\beta = 0$, and (b) $\beta = \alpha/4$.

tension parallel to the free surface also occurs for the bi-material case when $\omega = 45°$ and $\alpha = 0$. For an inclination ω close to 45° the level of singularity λ is modest, and the stress state at the interface-corner is predominantly shear parallel to the interface. The level of singularity λ also approaches unity for the case of a long and slender scarf joint, with ω close to 0°. We further note from Figure 2a that the stress state at the interface-corner is always less singular than the crack case ($\lambda = 0.5$) for the full range of ω and α. The solution is most singular for α close to unity for all values of ω, and for $\alpha \to -1$ with $45° < \omega \leqslant 90°$.

At the two opposing interface-corners of a scarf joint, the inclination ω is equal in magnitude but the mismatch parameter α jumps in sign. Consequently, the level of singularity is different at the two opposing interface-corners of the joint. For the purposes of the following discussion, we shall consider the lower material 2 to be stiffer than the upper material 1. Then, α is negative for the left-hand interface-corner and α is positive for the right-hand interface-corner of the joint, labelled A and B, respectively, in Figure 2(a). For ω less than 45°, the stress state is nonsingular at the left-hand corner and is singular at the right-hand interface-corner. For ω greater than 45° the left-hand corner is always singular; also, the right-hand corner is singular for a large value of material mismatch, but is nonsingular if α is sufficiently close to zero. For the limiting case of a butt joint ($\omega = 90°$), the stress states at both interface-corners of the strip are identical, and are singular for $\alpha \neq 0$.

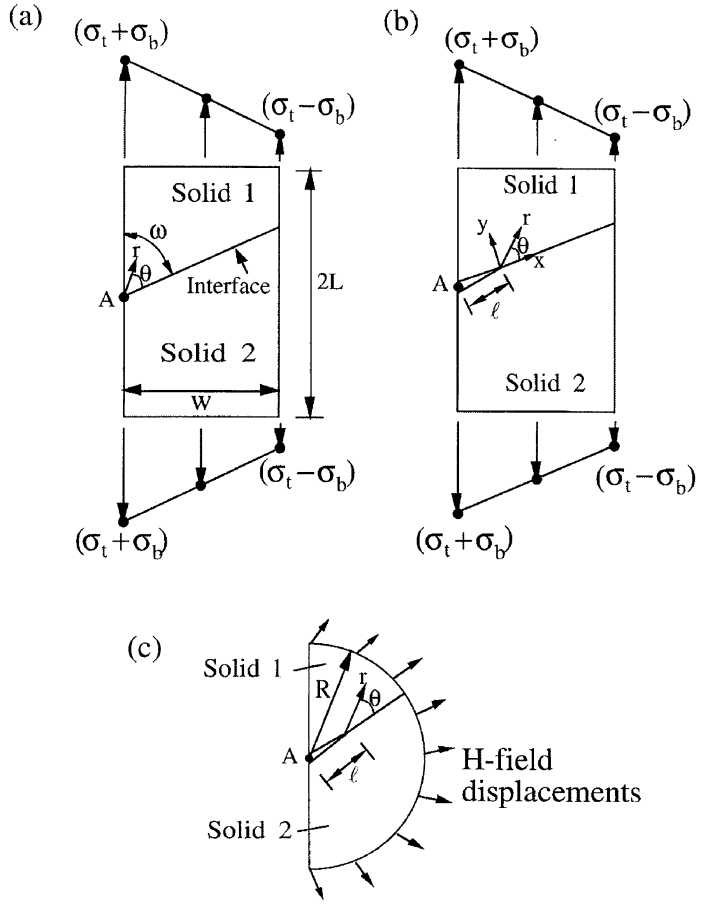

Figure 3. The bi-material geometries. (a) An uncracked bi-material strip with perfect adhesion between the two materials. (b) A bi-material strip with an interfacial edge crack of length ℓ. (c) A boundary layer geometry comprising a short interfacial edge crack embedded within the free-edge singular field.

Now consider the case $\beta = \alpha/4$, see Figure 2(b). In general, the contours of λ shift only slightly compared with the case $\beta = 0$. The horizontal line of $\lambda = 1$ shifts a little up the ω-axis to the location $\omega = 54.7°$. But there is an added complication. A small region now exists in the α, ω plane for which the stresses are singular and λ is complex. However, we note from Figure 2(b) that the imaginary part of λ is small. This region of complex singularity is thought to be of limited practical relevance, and is not considered further in our analysis.

1.2. Scope of the present study

We consider the scarf joint geometry shown in Figure 3(a). Two infinitely long strips, made from dissimilar isotropic elastic solids, are perfectly bonded along an interface oriented at an angle ω in the range 0–90° to the free surface. The strip, of width w is subjected to a remote uniform tensile stress σ_t giving rise to an axial tension P, or to a linear stress field of magnitude σ_b resulting in a bending moment M. The length $2L$ of the strip is assumed to be much greater than the width w, and so only the single length scale w enters the singularity analysis.

We shall calculate the intensity H of the free edge singularity that occurs at the left-hand interface-corner of the scarf joint (Figure 3(a)) due to remote tension and bending. In addition, we shall consider the case of a pre-existing edge crack of length ℓ along the interface, as shown in Figure 3(b). The interfacial stress intensity factor K (written in complex form as $K = K_1 + iK_2$, where $i = \sqrt{-1}$), and the nonsingular stress terms parallel to the crack surface (referred to as the 'T-stresses') are evaluated as functions of the relative crack length ℓ/w and elastic mismatch by the finite element method.

For the limiting case of small ℓ/w, the interfacial crack lies within the free-edge singularity characterised by H, and the interfacial K value is calculated in two steps as follows. First, the intensity H for the singular field is evaluated for the uncracked strip (Figure 3(a)) via a contour integral and the finite element method. Second, the stress intensity factor for a short interfacial crack lying within the H-field is extracted by solving an ancillary boundary layer problem which couples the inner K-field to the outer H-field. The boundary layer problem is solved by the finite element method and makes use of the geometry shown in Figure 3(c). The external semi-circular boundary of the domain is subjected to the displacements of the asymptotic H-field, and the interfacial stress intensity factor for the embedded crack is extracted using a J-integral evaluation. The paper concludes with a discussion of the effect of the interface orientation ω upon the initial growth of an interfacial crack, including a calculation of the strain energy release rate and the mode mix.

2. Formulation of the problem

2.1. Intensity H of the free-edge singularity

Let (r, θ) be cylindrical polar co-ordinates centred at the interface-corner A of the bi-material geometry shown in Figure 3(a). The singular field near the interface-corner is of the form

$$\sigma_{ij}^m = Hr^{\lambda-1} f_{ij}^m(\alpha, \beta, \omega, \theta),$$
$$u_i^m = \frac{1}{2\mu_m} Hr^{\lambda} g_i^m(\alpha, \beta, \omega, \theta) \tag{2.1}$$

where $(i, j) \equiv (r, \theta)$, $m(= 1, 2)$ is the material index, and f_{ij}^m and g_i^m are known functions of (ω, θ) and of the material mismatch parameters (α, β); explicit expressions for f_{ij}^m and g_i^m are given by Qian and Akisanya (1997a) and are not repeated here. We wish to evaluate H as a function of material elastic parameters (α, β) for remote tension of magnitude σ_t and for a bending stress field of magnitude σ_b, as shown in Figure 3(a).

The intensity H of the free-edge singularity will hereafter be referred to as the *free-edge intensity factor*. H is defined such that at a distance r from the interface-corner and along the interface ($\theta = 0$), the stress component normal to the interface, $\sigma_{\theta\theta}$, in the region dominated by the singularity is given by

$$\sigma_{\theta\theta}^1 = \sigma_{\theta\theta}^2 = Hr^{\lambda-1}, \tag{2.2}$$

where the superscripts 1 and 2 denote the two materials. The free-edge intensity factor H depends, in general, upon the free-edge geometry, elastic mismatch parameters and upon the

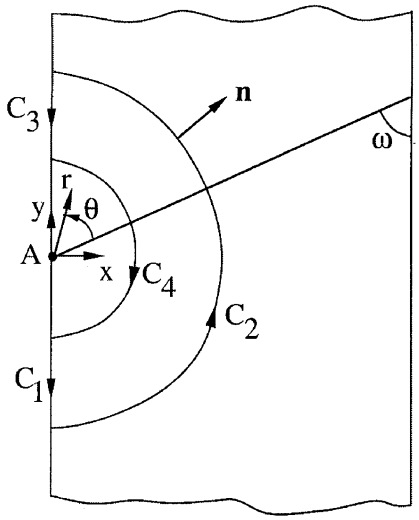

Figure 4. A closed integration path around the interface-corner A.

remote loading. Dimensional considerations dictate that H is related to the geometry and material elastic properties by

$$H = \sigma w^{1-\lambda}\mathbf{a}(\alpha, \beta, \omega) \tag{2.3}$$

where σ equals the remote tensile stress σ_t for remote tension and $\sigma = \sigma_b$ for remote bending, w is the width of the strip and **a** is a real dimensionless function of the elastic parameters α and β. Values for **a** are calculated using a contour integral method, based on Betti's reciprocal theorem; it involves a convolution of the asymptotic field of the corner singularity with a finite element solution. This contour integral method has been used by various authors to obtain the stress intensities for various crack and notch geometries, see for example, Stern et al. (1976), Sinclair et al. (1985), Carpenter and Byers (1987), and Akisanya and Fleck (1997). The method is based on Betti's reciprocal law (Sokolnikoff, 1956), and is outlined below.

Consider a closed contour $C(= C_1 + C_2 + C_3 + C_4)$ around the interface-corner A, as shown in Figure 4. Betti's reciprocal law can be stated as

$$\oint_C (\sigma_{ij}u_i^* - \sigma_{ij}^* u_i)n_j \, \mathrm{d}s = 0, \tag{2.4}$$

where $(i, j) \equiv (r, \theta)$ represent polar co-ordinates centred at the interface-corner, (σ_{ij}, u_i) are the free-edge singular stress and displacement fields given by (2.1), (σ_{ij}^*, u_i^*) are auxiliary fields satisfying the same boundary conditions as (σ_{ij}, u_i), n_j is the outward unit normal to C, and $\mathrm{d}s$ is an infinitesimal line segment of C. The integration in (2.4) is performed in an anticlockwise sense around C. By appropriate choice of the auxiliary field (σ_{ij}^*, u_i^*), the integral (2.4) can be used to determine the free-edge intensity factor H.

In the evaluation of H it is convenient to choose the auxiliary fields (σ_{ij}^*, u_i^*) as the free-edge singular stress and displacement fields given by (2.1) with intensity H^* and with λ replaced by $\lambda^* = -\lambda$. Then, the starred fields (σ_{ij}^*, u_i^*) satisfy the same boundary conditions as those for the unstarred fields (σ_{ij}, u_i). These boundary conditions are: (i) traction-free boundaries along $\theta = \omega - \pi$ and $\theta = \omega$, and (ii) continuity of displacements and stress components $(\sigma_{\theta\theta}, \sigma_{r\theta})$ along the interface, where (r, θ) are polar co-ordinates centred at the

interface-corner, as defined in Figure 3(a). The unstarred fields (σ_{ij}, u_i) are obtained for the bi-material strip geometry of Figure 3(a) using the finite element method. The value of the intensity H^* for the auxiliary field is chosen such that the evaluation of (2.4) by the contour integration method gives the intensity H for the elastic state of interest. A full description of the procedure for the evaluation of H is given in Appendix B of Akisanya and Fleck (1997), and is omitted here. Once the value of H has been obtained, we calculate the nondimensional constant $\mathbf{a}(\alpha, \beta, \omega)$ via (2.3).

Elastic analysis of the uncracked bi-material strip of Figure 3(a) has been carried out using the finite element code ABAQUS[1] The finite element mesh consists of 928 to 1564 eight-noded plane strain isoparametric, quadrilateral elements of the bi-material strip. The mesh near the interface-corner is refined in order to give adequate numerical accuracy in the vicinity of the singularity. The width of the strip w is taken as unity and the strip length $2L = 20w$. The results for the coefficient $\mathbf{a}$ are listed in Table 1 for both remote tension and remote bending, over the full range of practical values of the material parameters α and β, and of the inclination ω.

Table 1(a). Magnitude of $\mathbf{a}(\alpha, \beta = 0, \omega)$ for tension.

α	$\omega = 15°$	$\omega = 30°$	$\omega = 60°$	$\omega = 75°$	$\omega = 90°$
−0.99	0.0012	0.3211	0.4996	0.4365	0.3365
−0.8	0.0058	0.2911	0.5168	0.4879	0.4334
−0.5	0.0383	0.2789	0.5685	0.6010	0.6318
−0.2	0.0579	0.2631	0.6550	0.7729	0.8954
0.0	0.0670	0.2500	0.7500	0.9330	1.0000
0.2	0.0735	0.2353	0.9190	1.0444	0.8954
0.5	0.0758	0.2130	1.5676	0.7269	0.6318
0.8	0.0689	0.1924	0.3074	0.3819	0.4334
0.99	0.0663	0.1884	0.1167	0.2312	0.3365

Table 1(b). Magnitude of $\mathbf{a}(\alpha, \beta = \alpha/4, \omega)$ for tension.

α	$\omega = 15°$	$\omega = 30°$	$\omega = 45°$	$\omega = 60°$	$\omega = 75°$	$\omega = 90°$
−0.99	0.0010	0.0402	0.6410	0.6544	0.5647	0.4279
−0.8	0.0152	0.2461	0.6422	0.6633	0.6189	0.5472
−0.5	0.0374	0.2841	0.5948	0.6881	0.7400	0.7540
−0.2	0.0572	0.2671	0.5372	0.7220	0.8469	0.9476
0.0	0.0670	0.2500	0.5000	0.7500	0.9330	1.0000
0.2	0.0736	0.2312	0.4648	0.7830	0.9828	0.9476
0.5	0.0752	0.2017	0.4143	0.8332	0.8313	0.7540
0.8	0.0664	0.1683	0.3452	0.4423	0.4654	0.5472
0.99	0.0622	complex	0.2572	0.0807	0.2652	0.4279

[1] Hibbitt, Karlsson and Sorenson, ABAQUS Users Manual, Version 5.2, HKS Inc. (1992).

Table 1(c). Magnitude of $\mathbf{a}(\alpha, \beta = 0, \omega)$ for bending.

α	$\omega = 15°$	$\omega = 30°$	$\omega = 60°$	$\omega = 75°$	$\omega = 90°$
−0.99	0.00124	0.1121	0.1808	0.1945	0.2057
−0.8	0.0160	0.2309	0.2576	0.2676	0.3003
−0.5	0.0384	0.2600	0.3801	0.4188	0.5249
−0.2	0.0573	0.2601	0.5556	0.6716	0.8685
0.0	0.0670	0.2500	0.7500	0.9330	1.0000
0.2	0.0730	0.2300	1.1118	1.1898	0.8685
0.5	0.0744	0.2147	2.6836	0.8299	0.5249
0.8	0.0641	0.1868	0.6210	0.3751	0.3003
0.99	0.0601	0.1550	0.2140	0.2081	0.2057

Table 1(d). Magnitude of $\mathbf{a}(\alpha, \beta = \alpha/4, \omega)$ for bending.

α	$\omega = 15°$	$\omega = 30°$	$\omega = 45°$	$\omega = 60°$	$\omega = 75°$	$\omega = 90°$
−0.99	0.0011	0.0302	0.2346	0.2719	0.2868	0.2933
−0.8	0.0153	0.2311	0.3907	0.3694	0.3790	0.4209
−0.5	0.0378	0.2731	0.4803	0.5012	0.5458	0.6734
−0.2	0.0574	0.2665	0.5019	0.6409	0.7641	0.9348
0.0	0.0670	0.2500	0.5000	0.7500	0.9330	1.0000
0.2	0.0732	0.2314	0.4928	0.8843	1.0859	0.9348
0.5	0.0739	0.2015	0.4811	1.1891	0.9885	0.6734
0.8	0.0637	0.1703	0.5233	1.0651	0.5330	0.4209
0.99	0.0589	complex	0.3470	0.2952	0.2929	0.2933

2.2. STRESS INTENSITIES AND T-STRESSES FOR AN INTERFACIAL EDGE CRACK

If the interface of the scarf joint is sufficiently brittle in comparison with the two substrates, it is expected that failure will occur by the initiation and growth of an interfacial crack from the interface-corner. Therefore, an analysis of the stress state for an interfacial edge crack in the bi-material strip is of practical relevance; the precise geometry is given in Figure 3(b). Again, we consider the two loading cases of remote uniform tension, of magnitude σ_t, and a bending stress field of magnitude σ_b.

In general, an interfacial crack between two dissimilar isotropic elastic solids suffers a singular stress field characterised by the complex interfacial stress intensity factor $K = K_1 + iK_2$, where $i = \sqrt{-1}$. In order to define K we introduce the cylindrical polar co-ordinates (r, θ) placed at the crack tip as shown in Figure 3(b). Then, K is defined such that at a distance r directly ahead of the crack tip, the normal stress $\sigma_{\theta\theta}$ and shear stress $\sigma_{r\theta}$ are given by

$$\sigma_{\theta\theta} + i\sigma_{r\theta} = \frac{1}{\sqrt{2\pi}} K r^{-1/2+i\varepsilon} \tag{2.5}$$

where the oscillatory index ε depends only upon the material elastic mismatch parameter β via

$$\varepsilon = \frac{1}{2\pi} \ln\left(\frac{1-\beta}{1+\beta}\right). \tag{2.6}$$

In presenting the interfacial stress intensity solutions for both long and short edge cracks, it is convenient to define a phase angle ψ in relation to the crack length ℓ by

$$\tan\psi = \frac{\mathrm{Im}(K\ell^{i\varepsilon})}{\mathrm{Re}(K\ell^{i\varepsilon})}. \tag{2.7}$$

In the series expansion for the interfacial crack tip stress field, the next highest order term to the K field is given by in-plane direct stresses parallel to the crack plane. These stresses are of magnitude T_1 in material 1 and T_2 in material 2, and are referred to as the 'T-stresses'. Since the strain component ε_{rr} is the same on both sides of the interface, a direct relation exists between the T-stresses,

$$T_2 = \frac{1-\alpha}{1+\alpha}T_1. \tag{2.8}$$

When the cracked bi-material strip shown in Figure 3(b) is loaded by a stress σ (equal to σ_t for remote tension, and equal to σ_b for remote bending) the stress field at the tip of the interfacial crack of length ℓ from the free-edge is governed by the complex stress intensity factor K and the T-stresses, T_1 in material 1 and T_2 in material 2. Dimensional considerations require that the stress intensity factor and the T-stresses be related to the geometry and the applied stress σ by

$$K\ell^{i\varepsilon} = \sigma\sqrt{\ell}\,\mathbf{b}(\ell/w, \alpha, \beta, \omega) \tag{2.9}$$

and

$$T_1 = \sigma\mathbf{c}(\ell/w, \alpha, \beta, \omega). \tag{2.10}$$

We emphasise that $\sigma \equiv \sigma_t$ for the case of remote tensile loading, $\sigma \equiv \sigma_b$ for the case of remote bending; $\mathbf{b}(= b_1 + ib_2)$ is a complex nondimensional function and $\mathbf{c}$ is a real nondimensional function of the elastic mismatch parameters (α, β), of the inclination ω and of the relative crack length ℓ/w. We omit tables of values for $\mathbf{b}$ and $\mathbf{c}$ for the sake of brevity but will present relevant results in graphical form[2].

For the case where the interfacial edge crack of length ℓ lies within the zone of H-dominance the stress intensity factor and the T-stresses depend directly upon the magnitude of H. A boundary layer approach is used for evaluating the coupling between the crack tip parameters (K, T) and the free-edge singularity parameter H. The boundary layer geometry shown in Figure 3(c) is loaded on the semi-circular boundary by the asymptotic free-edge displacement field characterised by H (Equation (2.1)).

The interfacial stress intensity factor K has the dimension (stress)(length)$^{1/2-i\varepsilon}$, while the free-edge intensity factor H has the dimension (stress)(length)$^{1-\lambda}$. Dimensional considerations require that the interfacial stress intensity factor K and the T-stress T_1 in material 1 be related to the geometry and the free-edge intensity factor H by

$$K\ell^{i\varepsilon} = H\ell^{\lambda-1/2}\mathbf{d}(\alpha, \beta, \omega), \tag{2.11}$$

[2] We note in passing that the **b**-values for the butt joint presented in Table 2 of Akisanya and Fleck (1997) require correction: entries in the table should be multiplied by the factor $(10\ell/w)^{i\varepsilon-(1/2)}$.

and

$$T_1 = H\ell^{\lambda-1}\mathbf{e}(\alpha, \beta, \omega). \tag{2.12}$$

Here, $\mathbf{d}$ $(= d_1 + id_2)$ is a complex nondimensional function and $\mathbf{e}$ is a real nondimensional function of the elastic mismatch parameters α and β and of the inclination ω; the evaluation of these functions is described in the following sub-section.

By substituting the expression (2.3) for the free-edge intensity factor H into (2.11) and (2.12), the interfacial stress intensity factor K and the T-stress T_1 in material 1 for an interfacial crack embedded within the free-edge singularity zone are given in terms of the remote loading σ, crack length ratio ℓ/w and material parameters (α, β) by

$$K\ell^{i\varepsilon} = \sigma\sqrt{\ell}\left(\frac{\ell}{w}\right)^{\lambda-1}\mathbf{a}(\alpha, \beta, \omega)\,.\,\mathbf{d}(\alpha, \beta, \omega), \tag{2.13}$$

and

$$T_1 = \sigma\left(\frac{\ell}{w}\right)^{\lambda-1}\mathbf{a}(\alpha, \beta, \omega)\,.\,\mathbf{e}(\alpha, \beta, \omega). \tag{2.14}$$

2.3. Numerical evaluation of interfacial stress intensity factor and T-stress

The interfacial stress intensity factor K and the T-stresses for a crack of length ℓ laying on the interface of the scarf joint are determined by:

(i) evaluating the path-independent J-integral for the cracked geometry, loaded by remote tension or bending, followed by
(ii) evaluating the J-integral for the same cracked geometry, with a suitably-chosen auxiliary elastic field superimposed on the remote loading.

Parks' (1974) virtual crack extension method is used to evaluate the path independent J-integral. For the evaluation of the components K_1 and K_2 of the interfacial stress intensity factor, the auxiliary field is taken to be the singular crack tip field for an interfacial crack, as described by Matos et al. (1989). In the evaluation of the T-stresses, the auxiliary elastic field consists of a point force placed at the tip of a semi-infinite interfacial crack and in a direction parallel to the crack faces. A detailed description of these methods is given by Akisanya and Fleck (1994).

Finite element analysis is again carried out using the finite element code ABAQUS. The finite element mesh contains 1354 to 1728 elements for the case of long crack (Figure 3(b)) and 638 elements for the boundary layer problem (Figure 3(c)). In all cases eight-noded plane strain isoparametric, quadrilateral elements are used. The numerically obtained values for the coefficients $\mathbf{d}$ and $\mathbf{e}$ are listed in Tables 2 and 3, for various values of material parameters α and $\beta(= 0$ and $\alpha/4)$, and interface orientation ω. Numerical experimentation suggests that the results for K and T_1 are accurate to within about 1 percent.

3. Results

3.1. Magnitude of the free edge intensity factor H

The magnitude of the free-edge intensity factor H is related to the applied stress σ ($\sigma = \sigma_t$ for tension and $\sigma = \sigma_b$ for bending), the strip width w, the joint inclination ω and the material elastic properties (α, β) in the manner given by (2.3). The nondimensional real parameter $\mathbf{a}(\alpha, \beta, \omega)$ is determined by the contour integral method as described in Section 2.1 and detailed in Appendix B of Akisanya and Fleck (1997). Values for **a** are listed in Table 1 for the tensile and bending cases, over the full range of values for α, and for the two values, $\beta = 0$ and $\alpha/4$. Contours of the nondimensional measure **a** of the intensity factor H are plotted as a function of material parameter α and joint inclination ω in Figure 5(a) for the case $\beta = 0$ and in Figure 5(b) for the case $\beta = \alpha/4$.

For both remote tension and bending and for all (α, β) considered, **a** increases from zero as ω increases from zero, see Figures 5(a, b). For $\omega < 30°$, **a** remains small (less than 0.3) and is relatively insensitive to the value of (α, β) and to the nature of the remote loading; for larger values of ω, the behaviour is more complicated and the precise value of **a** depends upon (α, β) and upon the type of remote loading. We note that **a** is complex (and has not been evaluated) within the same small domain of (α, β) values for which λ is complex. For the limiting case of a butt joint under remote tension ($\omega = 90°$), Akisanya and Fleck (1997) showed that a unique correlation exists between **a** and λ for all (α, β) considered. No such correlation is observed here for $\omega \neq 90°$. Numerical experimentation and a comparison of the results given by Qian and Akisanya (1997a) for the scarf joint under remote tension suggest that the values of **a** in the current study are accurate to within 1 percent.

3.2. Zone of dominance of the free-edge singularity

It is important to determine the physical size of the singularity zone in relation to the width w of the bi-material strip in order to appraise whether the intensity of singularity H can be used as a failure criterion. The intensity H is expected to be a useful parameter provided the fracture process zone and any nonlinear plastic zone at the interface-corner are fully embedded within the elastic H-field. The finite element results are compared with the asymptotic solution in Figure 6 by plotting the stress components $(\sigma_{\theta\theta}, \sigma_{r\theta})$ along the interface against the radial distance r from the left hand interface-corner A, for the selected cases $\omega = 30°$ and $\omega = 90°$, and $\alpha = 0.5, \beta = \alpha/4$. First, consider the butt joint, $\omega = 90°$; the asymptotic results are adequate (i.e. lay within 5 percent of the finite element values) for r/w extending out to 0.01 in the bending case, and to 0.03 in the tensile case. Second, consider the inclination $\omega = 30°$; the asymptotic results are within 5 percent of the finite element results for r/w extending to 0.07 in both the bending and tensile cases. Numerical experimentation reveals that these findings are relatively insensitive to the material mismatch parameters (α, β). We conclude that the singular zone extends across a significant fraction of the strip, particularly for the loading case of remote tension. Akisanya and Fleck (1997) and Qian and Akisanya (1997a) drew similar conclusions from their studies on the free-edge singularity at a butt joint ($\omega = 90°$) under remote tension, and at a scarf joint under remote tension, respectively.

Table 2(a). Values of $\mathbf{d} = d_1 + id_2$ for $\beta = 0$.

α		$\omega = 15°$	$\omega = 30°$	$\omega = 60°$	$\omega = 90°$
−0.99	d_1	6.2312	2.7684	2.6714	2.2803
	d_2	4.6028	1.1213	0.9539	0.6468
−0.8	d_1	6.3063	3.0009	2.5898	2.2639
	d_2	4.8353	1.4391	0.9203	0.5991
−0.5	d_1	6.2465	3.1601	2.4383	2.0957
	d_2	5.1711	1.7968	0.8616	0.4109
−0.2	d_1	6.1762	3.2460	2.2730	1.9611
	d_2	5.6044	2.1391	0.7852	0.1831
0.0	d_1	6.1156	3.2600	2.1582	1.9241
	d_2	5.9673	2.3702	0.7184	0.0000
0.2	d_1	6.0540	3.2637	2.0231	1.9611
	d_2	6.4357	2.6329	0.6192	−0.1831
0.5	d_1	5.8485	3.1658	1.8281	2.0957
	d_2	7.3701	3.0659	0.2821	−0.4109
0.8	d_1	5.1891	2.8355	2.2328	2.2639
	d_2	8.8061	3.6076	−0.2660	−0.5991
0.99	d_1	3.0292	2.0912	2.3127	2.2803
	d_2	10.3894	4.1046	−0.4994	−0.6468

Table 2(b). Values of $\mathbf{d} = d_1 + id_2$ for $\beta = \alpha/4$.

α		$\omega = 15°$	$\omega = 30°$	$\omega = 60°$	$\omega = 90°$
−0.99	d_1	4.6127	2.2327	2.2176	2.3259
	d_2	6.3703	1.6322	1.0330	0.6793
−0.8	d_1	4.8996	2.4707	2.2125	2.1911
	d_2	6.2074	1.8432	0.9619	0.5620
−0.5	d_1	5.6410	2.7821	2.2570	2.0343
	d_2	5.9206	2.0482	0.8617	0.3558
−0.2	d_1	5.7932	3.0788	2.1779	1.9426
	d_2	5.9303	2.2371	0.7702	0.1404
0.0	d_1	6.1156	3.2600	2.1582	1.9241
	d_2	5.9673	2.3702	0.7184	0.0000
0.2	d_1	6.4834	3.4516	2.1257	1.9426
	d_2	6.1322	2.5464	0.6668	−0.1404
0.5	d_1	7.0342	3.6711	2.0893	2.0343
	d_2	6.6811	2.9049	0.5938	−0.3558
0.8	d_1	7.2927	3.6697	2.0563	2.1911
	d_2	8.0678	3.6275	0.2955	−0.5620
0.99	d_1	5.5262	complex	2.2478	2.3259
	d_2	14.9905	complex	−0.1492	−0.6793

Table 3(a). Magnitude of $\mathbf{e}(\alpha, \beta = 0, \omega)$.

α	$\omega = 15°$	$\omega = 30°$	$\omega = 60°$	$\omega = 90°$
−0.99	9.0868	0.0703	−0.0005	−0.0049
−0.8	9.8381	0.7260	−0.0106	−0.0984
−0.5	10.9850	1.4867	−0.0363	−0.2511
−0.2	12.4639	2.2471	−0.0814	−0.4100
0.0	13.6886	2.7836	−0.1311	−0.5109
0.2	15.2441	3.3916	−0.2117	−0.6150
0.5	18.3923	4.4427	−0.5514	−0.7532
0.8	23.4519	5.8481	−1.1748	−0.8852
0.99	30.4237	7.2838	−1.4929	−0.9741

Table 3(b). Magnitude of $\mathbf{e}(\alpha, \beta = \alpha/4, \omega)$.

α	$\omega = 15°$	$\omega = 30°$	$\omega = 60°$	$\omega = 90°$
−0.99	9.7696	0.4853	−0.0018	−0.0050
−0.8	10.4107	0.9419	−0.0344	−0.1000
−0.5	11.4073	1.5610	−0.0770	−0.2521
−0.2	12.5068	2.2519	−0.1132	−0.4075
0.0	13.6886	2.7836	−0.1311	−0.5109
0.2	15.2893	3.4308	−0.1437	−0.6112
0.5	18.7599	4.6783	−0.1674	−0.7564
0.8	25.0216	6.7842	−0.4127	−0.8998
0.99	49.0327	complex	−0.8623	−0.9947

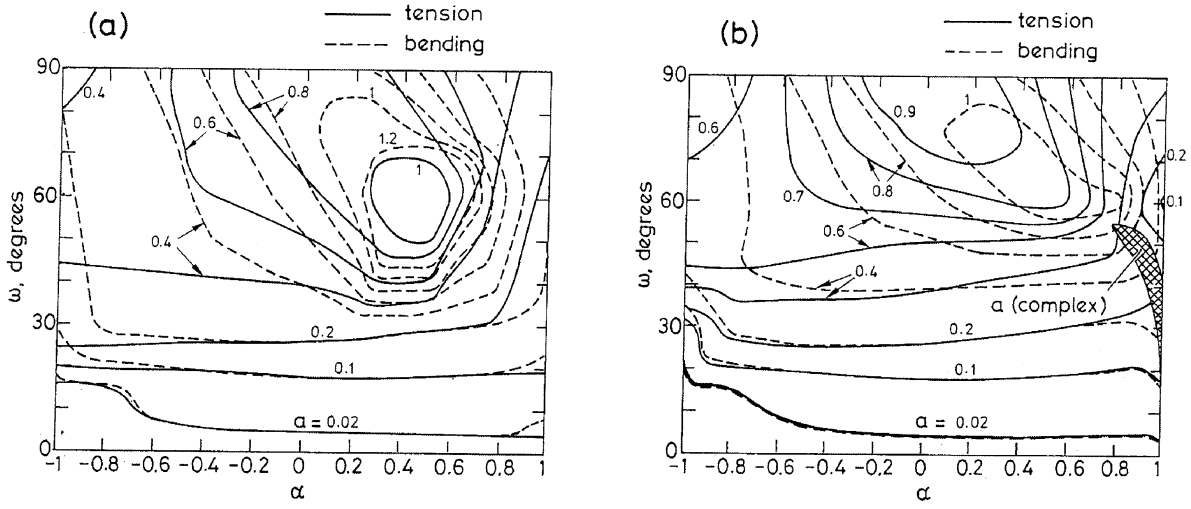

Figure 5. Contours of **a** as a function of α and joint inclination ω, for both remote tension and remote bending. (a) $\beta = 0$ and (b) $\beta = \alpha/4$.

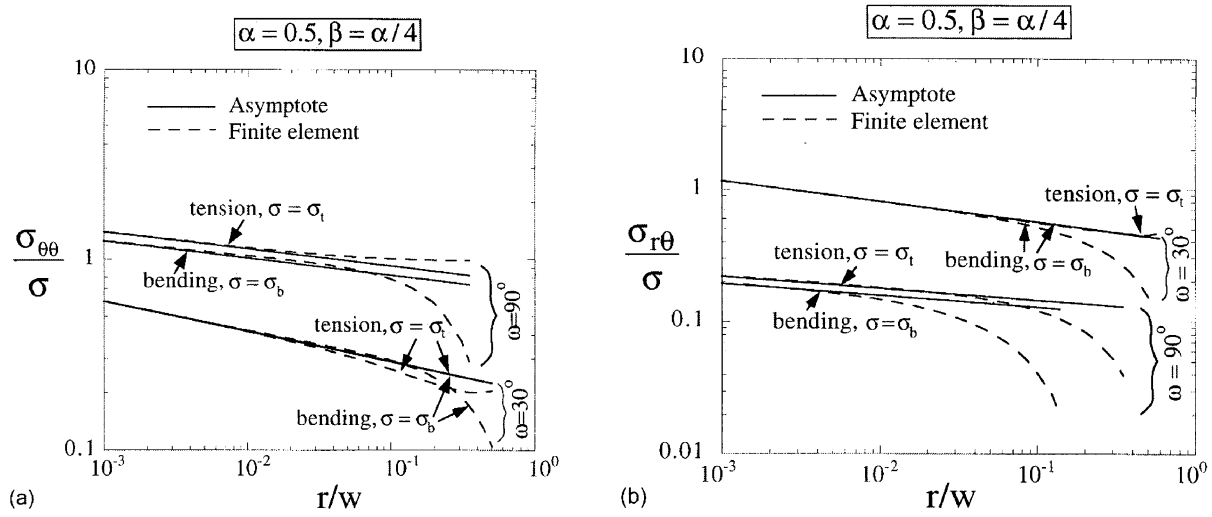

Figure 6. A comparison of the finite element and asymptotic solutions for the traction on the interface, as a function of distance r from the interface-corner. $\alpha = 0.5$ and $\beta = \alpha/4$. (a) $\sigma_{\theta\theta}/\sigma$ versus r/w, and (b) $\sigma_{r\theta}/\sigma$ versus r/w, where $\sigma \equiv \sigma_t$ for remote tension and $\sigma \equiv \sigma_b$ for remote bending.

3.3. Interfacial stress intensity factor

The nondimensional real and imaginary parts of the complex interfacial stress intensity factor defined by (2.9) and (2.13) are plotted in Figures 7(a, b) for $\alpha = 0.5$, $\beta = \alpha/4$, and in Figures 7(c, d) for $\alpha = -0.5$, $\beta = \alpha/4$. Results are shown for selected values of joint inclination, $\omega = 15°, 30°, 60°$ and $90°$. The values for K have been normalised by $\sigma\sqrt{\ell}$ where $\sigma = \sigma_t$ for the tensile case and $\sigma = \sigma_b$ for the bending case, in order to elucidate the significance of the corner singularity on K. The stress intensity factor values shown for $\ell/w \leqslant 0.01$ are the asymptotic results for a crack embedded within the free-edge singularity zone (see Figure 3(c)); results for $\ell/w \geqslant 0.06$ correspond to a long interfacial crack and are determined by finite element analysis of the cracked strip shown in Figure 3(b). Linear interpolation is used within the intermediate regime, $0.01 < \ell/w < 0.06$.

In order to provide a baseline reference for the magnitude of K recall that for the homogeneous case ($\alpha = \beta = 0$) with $\omega = 90°$, we have $K_1 = \mathrm{Re}(K\ell^{i\varepsilon}) = 1.12\sigma\sqrt{\pi\ell} = 1.985\sigma\sqrt{\ell}$ and $K_2 = \mathrm{Im}(K\ell^{i\varepsilon}) = 0$. It is evident from Figures 7(a–d) that the interfacial stress intensity factor for short crack lengths ($\ell/w < 0.1$) is amplified when the stress field at the interface-corner has an unbounded singularity. The magnitude of the normalised stress intensity factor increases with decreasing crack length within the singularity region. This result can be deduced directly from (2.13): the magnitude of $K\ell^{i\varepsilon}/\sigma\sqrt{\ell}$ scales with $(\ell/w)^{\lambda-1}$. Now consider the opposite limit, $\ell/w \to 1$. In all cases there is a sharp up-turn in the magnitude of $K\ell^{i\varepsilon}/\sigma\sqrt{\ell}$ as $\ell/w \to 1$; it is clear from a separate asymptotic analysis that $(K\ell^{i\varepsilon}/\sigma\sqrt{\ell}) \to \infty$ as $\ell/w \to 1$.

There is no simple monotonic dependence of $K\ell^{i\varepsilon}$ upon the inclination ω. It is clear, however, that $K\ell^{i\varepsilon}$ has the largest real values for the limiting case of a butt joint, $\omega = 90°$. If the inclination of the interface ω is less than about 30°, both the real and imaginary components of the interfacial stress intensity factor decrease with decreasing ω at a constant ℓ/w: the inter-

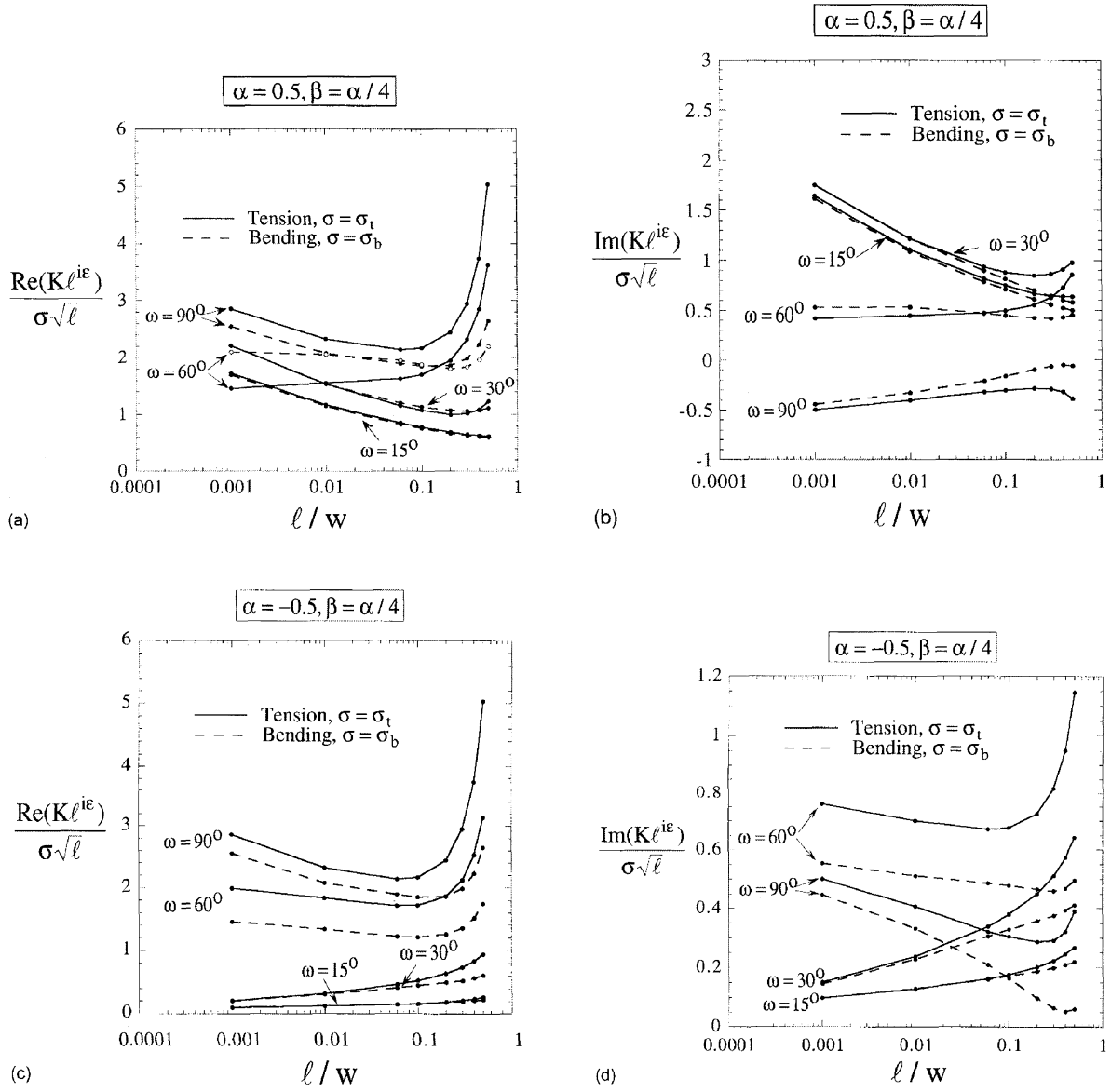

Figure 7. The effect of the interface orientation ω and relative crack length ℓ/w upon the interfacial stress intensity factor, for the case $\beta = \alpha/4$ (a) $[\mathrm{Re}(K\ell^{i\varepsilon})]/\sigma\sqrt{\ell}$ versus ℓ/w for $\alpha = 0.5$; (b) $[\mathrm{Im}(K\ell^{i\varepsilon})]/\sigma\sqrt{\ell}$ versus ℓ/w for $\alpha = 0.5$; (c) $[\mathrm{Re}(K\ell^{i\varepsilon})]/\sigma\sqrt{\ell}$ versus ℓ/w for $\alpha = -0.5$; and (d) $[\mathrm{Im}(Kl^{i\varepsilon})]/\sigma\sqrt{l}$ versus ℓ/w for $\alpha = -0.5$.

facial stress intensity factor tends to zero as ω tends to zero. Examination of the representative cases shown in Figure 7(a–d) shows that the nature of the remote loading (bending versus tension) has a greater effect on the interfacial stress intensity factor at larger values of ω, for both short and long cracks.

The real and imaginary components of the stress intensity factor $K\ell^{i\varepsilon}$ are positive in all cases shown in Figure 7(a–d) with the following exception: the imaginary part of $K\ell^{i\varepsilon}$ is negative for $\omega = 90°$, $\alpha = 0.5$, $\beta = \alpha/4$ for both tensile loading and bending, as shown in Figure 7(b). A positive value of the real part of $K\ell^{i\varepsilon}$ implies that the crack is open (except over a very small segment behind the crack tip due to the oscillatory nature of the crack singularity),

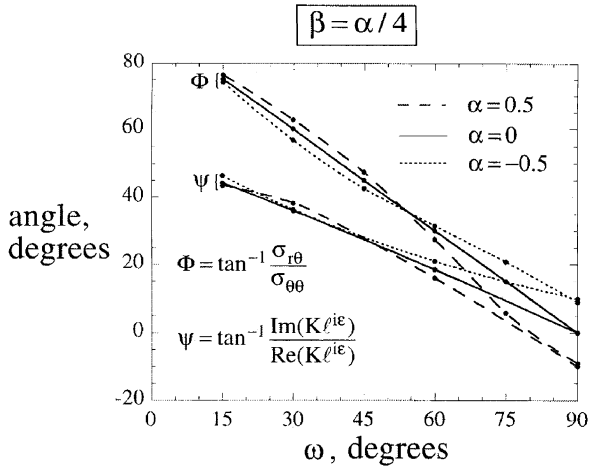

Figure 8. The phase angle $\psi \equiv \arctan[\mathrm{Im}(K\ell^{i\varepsilon})/\mathrm{Re}(K\ell^{i\varepsilon})]$ for an interfacial crack embedded within the interface-corner singular field, and the phase angle $\Phi \equiv \arctan[\sigma_{r\theta}/\sigma_{\theta\theta}]$ for the corner singularity in the absence of a crack, as a function of joint inclination ω. $\alpha = -0.5$, 0 and 0.5, with $\beta = \alpha/4$.

and a positive value of the imaginary part of $K\ell^{i\varepsilon}$ implies that the interfacial crack has a tendency to kink out of the interface into the lower material 2, provided the toughness of material 2 is sufficiently low in comparison with the interfacial toughness. The phase angle $\psi \equiv \arctan[\mathrm{Im}(K\ell^{i\varepsilon})/\mathrm{Re}(K\ell^{i\varepsilon})]$ for an interfacial crack embedded within the interface-corner singular field is shown in Figure 8 as a function of inclination ω, for $\alpha = -0.5$, 0 and 0.5, and $\beta = \alpha/4$. For the case $\alpha = \beta = 0$, the phase angle decreases with increasing ω in an almost linear manner, from a value $\psi = 44.3°$ at $\omega = 15°$ to a value $\psi = 0°$ at $\omega = 90°$. The effect of the value of the material mismatch parameters on the phase angle is minor provided ω is less than about 45°, but becomes significant for larger values of ω.

It is of interest to compare the phase angle of the interfacial stress intensity factor with the phase angle of the traction on the interface, associated with the corner singularity (in the absence of a crack). For the corner-singularity, the traction on the interface comprises a shear traction $\sigma_{r\theta}$ and a normal traction $\sigma_{\theta\theta}$, and the ratio of shear traction to normal traction $\sigma_{r\theta}/\sigma_{\theta\theta}$ of the asymptotic solution can be characterised by the phase angle $\Phi \equiv \arctan(\sigma_{r\theta}/\sigma_{\theta\theta})$. The dependence of the angle Φ upon the inclination ω is included in Figure 8, for selected values of α with $\beta = \alpha/4$. For the case $\alpha = \beta = 0$, the singularity vanishes and $\Phi = 90° - \omega$. The value of Φ changes slightly for the general bi-material case with $\alpha \neq 0$. For $\omega = 90°$, geometric symmetry dictates that the phase angle ψ of the stress intensity factor for a short interfacial crack equals the phase angle Φ of the traction on the interface; in the general case, $\omega \neq 90°$, Φ increases with decreasing ω at a faster rate than does ψ. Thus, for small values of ω the relative amount of shear to normal traction on a crack-free interface is significantly higher than the relative mode II to mode I stress intensity for a short interfacial crack.

3.4. THE INTERFACIAL T-STRESS

The magnitude and sign of the T-stress can affect the kinking behaviour of an interfacial crack out of the interface (He et al., 1991; Akisanya and Fleck, 1994). A positive value of T-stress both encourages kinking of an interfacial crack and causes the kinked crack to grow unstably under fixed remote load. In addition, the subsequent trajectory of the kink is expected

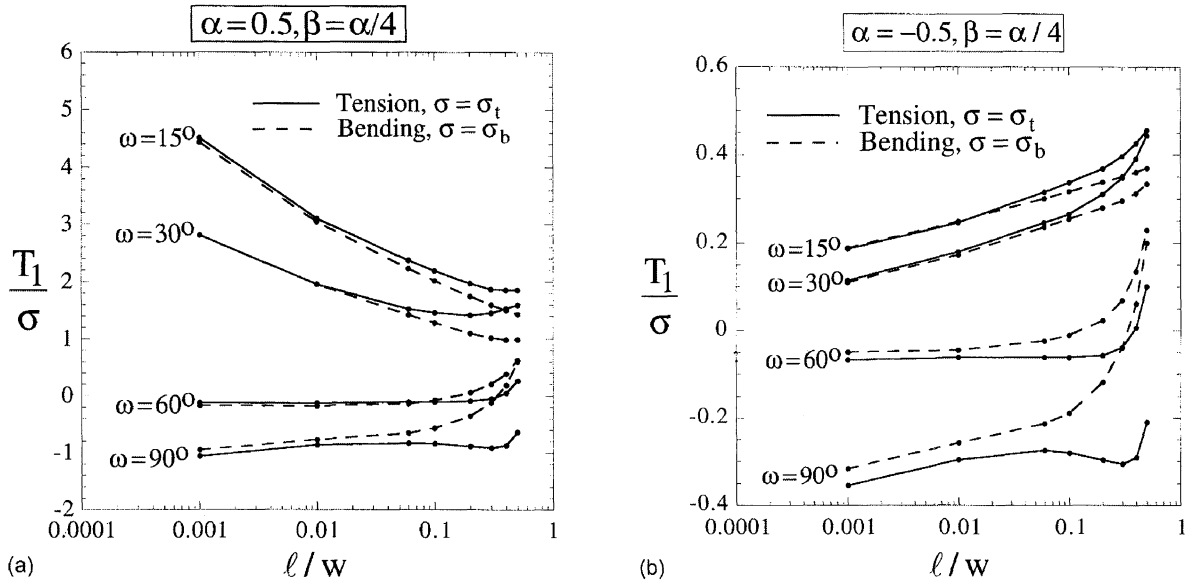

Figure 9. The effect of the interface orientation ω and relative crack length ℓ/w upon the T-stress in material 1, for $\beta = \alpha/4$. (a) $\alpha = 0.5$ and (b) $\alpha = -0.5$.

to diverge from the interface if the T-stress is positive (Cotterell and Rice, 1980). A negative value of the T-stress has the following effects:

(i) it stabilises an interfacial crack against kinking,
(ii) it may cause a kinked crack to arrest, and
(iii) crack growth from an initial kink is expected to converge towards the interface.

Figure 9 shows the normalised T-stress, T_1/σ, in material 1 due to remote tensile loading $\sigma = \sigma_t$, and due to remote bending of amplitude $\sigma = \sigma_b$, as a function of relative crack length ℓ/w. Results are shown for $\alpha = \pm 0.5$ and $\beta = \alpha/4$. Values are calculated directly by the finite element method for long interfacial cracks of geometry shown in Figure 3(b), and as described in Section 2.3. For the case of short interfacial cracks ($\ell/w \leqslant 0.01$), embedded within the corner singularity, the magnitude of T_1/σ is calculated in two steps as detailed in Section 2.2:

(i) calculation of the magnitude of H for the geometry of Figure 3(a), and
(ii) calculation of the coupling between H and T_1 for the boundary layer geometry of Figure 3(c).

Thus, results for T_1 in Figure 9 are taken from (2.10) for $\ell/w \geqslant 0.06$ and are taken from (2.14) for $\ell/w \leqslant 0.01$. Intermediate values of ℓ/w, $0.01 < \ell/w < 0.06$, are derived by linear interpolation.

The level of T-stress is relatively insensitive to the nature of the remote loading for short interfacial cracks and $\omega \leqslant 30°$, as shown in Figure 9. This is obvious from an examination of (2.10): for short interfacial cracks the only dependence of H upon type of loading is via the nondimensional parameter **a**. Provided $\omega \leqslant 30°$, **a** is not strongly influenced by the nature of the remote loading (see Figure 5(a, b)). When the interfacial crack is of comparable length to

the specimen width, the T-stress increases with increasing ℓ/w, and depends significantly upon the nature of the remote loading. For all lengths of interfacial crack considered, T_1 increases with diminishing ω. For example, for a short interfacial crack $\ell/w = 10^{-3}$ and $\alpha = 0.5$, T_1/σ increases from a value of about -1 at $\omega = 90°$ to $T_1/\sigma = 4.5$ at $\omega = 15°$, for both remote tension and remote bending. We further note from Figures 9(a, b) that, for short cracks, the sign of the T-stress switches from a negative value for joint inclinations ω close to the butt joint geometry ($\omega = 90°$) to a positive value at smaller values of ω.

3.5. Strain energy release rate and phase angle

The normalised strain energy release rate $E^*G_1/\sigma^2 w$ is given by

$$\frac{E^*G_1}{\sigma^2 w} = \left(\frac{\ell}{w}\right)^{2\lambda-1} \mathbf{a}^2(d_1^2 + d_2^2) \tag{3.1}$$

for an interfacial crack within the free-edge singularity zone, and by

$$\frac{E^*G_1}{\sigma^2 w} = \left(\frac{\ell}{w}\right)(b_1^2 + b_2^2) \tag{3.2}$$

for an interfacial crack whose tip is outside the singularity region. Here, $E^* \equiv (1+\alpha)E_2/[(1-\beta^2)(1-\nu_2^2)]$, where E_2 and ν_2 are the Young's modulus and the Poisson's ratio of material 2 below the interface. The corresponding phase angle of loading at the crack tip ψ defined by (2.7) is obtained from (2.11) or (2.13). Once the calibration functions $\mathbf{a}(\alpha, \beta)$, $\mathbf{b}$ $(\ell/w, \alpha, \beta)$ and $\mathbf{d}$ (α, β) have been deduced from the finite element analysis, the quantities G_1 and ψ are known for any prescribed remote loading σ and strip width w. Recall that the coefficient $\mathbf{a}$ is real while the coefficients $\mathbf{b}$ and $\mathbf{d}$ are complex functions: we restrict our attention to real values of the singularity level λ.

Results for $E^*G_1/\sigma^2 w$ and ψ are given in Figures 10(a) and (b) for the case $\alpha = 0.5$, and in Figures 10(c) and (d) for $\alpha = -0.5$. Each curve is for a prescribed value of inclination ω and results are shown for both remote tension and remote bending. The inclination ω has a major effect upon both the level of energy release rate G_1 for a given crack length and upon the phase angle ψ. The details of the remote loading become increasingly important with crack extension, as commented upon previously.

The normalised strain energy release rate $E^*G_1/\sigma^2 w$ increases monotonically from zero as the crack length is increased, with a relatively small attendant change in the phase angle ψ. This suggests that interfacial crack growth from the free edge is unstable under fixed remote loading. The effect of the material elastic mismatch parameter β upon the values of $E^*G_1/\sigma^2 w$ and ψ is minor.

4. Concluding remarks

A singularity of the type $Hr^{\lambda-1}$ exists at the free-edge of a scarf joint between two dissimilar elastic solids under remote tension and remote bending. In this paper we have presented a finite element analysis for the evaluation of the intensity H and of the order of the stress singularity $\lambda - 1$. For almost all values of material mismatch in the practical range, the eigenvalue λ is real. The intensity H is evaluated by a contour integral method. The singular zone extends to a distance of about $0.03w$ from the interface corner, where w is the width of the bi-material

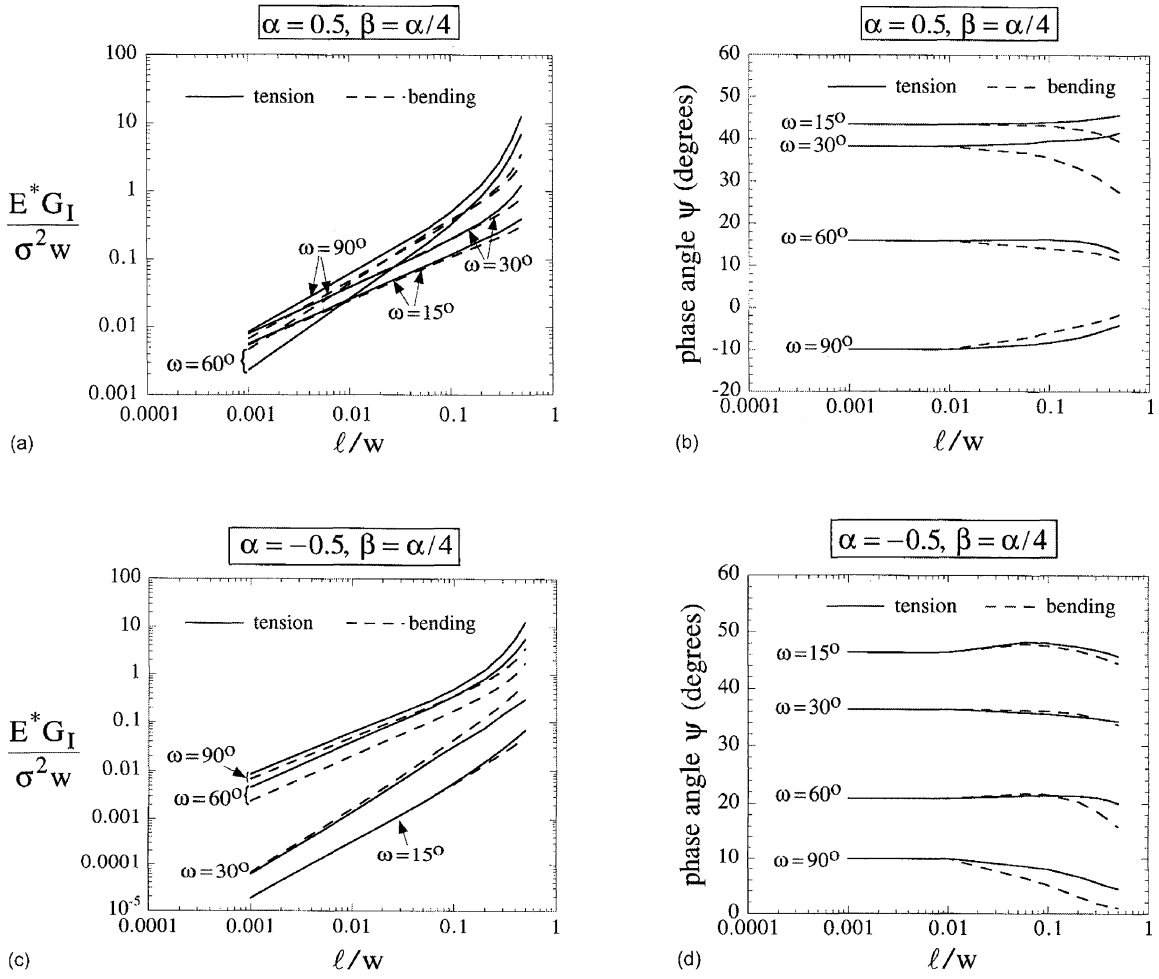

Figure 10. The effect of the interface orientation ω and relative crack length ℓ/w upon the nondimensional energy release rate $E^*G_I/\sigma^2 w$ and the phase angle $\psi = \arctan[\mathrm{Im}(K\ell^{i\varepsilon})/\mathrm{Re}(K\ell^{i\varepsilon})]$ for $\beta = \alpha/4$. (a) $E^*G_I/\sigma^2 w$ vs. ℓ/w, and (b) ψ vs. ℓ/w for $\alpha = 0.5$; (c) $E^*G_I/\sigma^2 w$ vs. ℓ/w, and (d) ψ vs. ℓ/w for $\alpha = -0.5$.

strip. It is expected that H provides a useful correlating parameter for fracture initiation at the free edge of the scarf joint.

Experimental data are not yet available to verify (or refute) the use of a critical value for H as a fracture initiation criterion for scarf joints. This approach suggests that the strength of a scarf joint scales with the width w of the panel to the power (λ-1) where λ depends upon both the material mismatch and the inclination of the scarf joint. In general λ is greater than 0.5 and so the expected size dependence is weaker than that for a cracked structure.

In the finite element evaluation of the free-edge intensity factor H for the uncracked bi-material strip we have taken the length L to equal $20w$, where w is the width of the strip. Numerical experimentation shows that this ratio of L/w is sufficiently large for the results to be independent of L: the numerical results pertain to the case of a long strip, with w as the only length-scale in the problem.

A calibration of the interfacial stress intensity factor K and the T-stress is given for a crack lying within the singularity region and also for a crack whose tip is outside the singularity

zone. There is a significant effect of the H-singularity field on the magnitude of the stress intensity factor and upon the T-stress for the crack. The energy release rate for the interfacial edge crack increases monotonically with crack extension: it is expected that an interfacial crack will grow unstably under fixed load.

Acknowledgements

Financial support is gratefully acknowledged from the EPSRC and from the Office of Naval Research (contract 0014-91-J-1916).

References

Akisanya, A.R. and Fleck, N.A. (1994). The edge cracking and decohesion of thin films. *International Journal of Solids and Structures* **31**, 3175–3199.

Akisanya, A.R. and Fleck, N.A. (1997). Interfacial cracking from the free edge of a long bi-material strip. *International Journal of Solids and Structures* **34**, 1645–1665.

Bazant, Z.P. (1997). Scaling of quasibrittle fracture: Asymptotic analysis. *International Journal of Fracture* **83**, 19–40.

Bogy, D.B. (1971). Two edge-bonded elastic wedges of different materials and wedge angles under surface tractions. *Journal of Applied Mechanics* **38**, 377–386.

Carpenter, W.C. and Byers, C. (1987). A path independent integral for computing stress intensities for V-notched cracks in bi-materials. *International Journal of Fracture* **35**, 245–268.

Carpinteri, A. (1996). Strength and toughness in disordered materials: Complete and incomplete singularity. *Size-Scale Effects in the Failure Mechanisms of Materials and Structures* (Edited by A. Carpinteri), E & FN Spon, 3–26.

Cotterell, B. and Rice, J.R. (1980). Slightly curved or kinked cracks. *International Journal of Fracture* **16**, 155–169.

Dundurs, J. (1969). *Mathematical Theory of Dislocations*. American Society of Mechanical Engineers, New York.

Gradin, P.A. (1982). A fracture criterion for edge-bonded bi-material bodies. *Journal of Composite Materials* **16**, 448–456.

Groth, H. L. (1988). Stress singularities and fracture at interface-corners in bonded joints. *International Journal of Adhesion and Adhesives* **8**, 107–113.

Groth, H.L. and Brottare, I. (1988). Evaluation of singular intensity factors in elastic-plastic materials. *Journal of Testing and Evaluation* **16**, 291–297.

Hattori, T., Sakata, S. and Murakami, G. (1989). A stress singularity parameter approach for evaluating the interfacial reliability of plastic encapsulated LSI devices. *Journal of Electronic Packaging* **111**, 243–248.

He, M.Y., Bartlett, A., Evans A.G. and Hutchinson, J.W. (1991). Kinking of a crack out of an interface: Role of in-plane stress. *Journal of American Ceramic Society* **74**, 767–771.

Hein, V.L. and Erdogan, F. (1971). Stress singularities in a two-material wedge. *International Journal of Fracture Mechanics* **7**, 317–330.

Kinloch, A.J. (1987). *Adhesion and Adhesives*. Chapman and Hall.

Matos, P.P.L., McMeeking, R.M., Charalambides, P.G. and Drory, M.D. (1989). A method for calculating stress intensities in bi-material fracture. *International Journal of Fracture* **40**, 235–254.

Munz, D. and Yang, Y.Y. (1992). Stress singularities at the interface in bonded dissimilar materials under mechanical and thermal loading. *Journal of Applied Mechanics* **59**, 857–861.

Munz, D. and Yang, Y.Y. (1993). Stress near the edge of bonded dissimilar materials described by two stress factors. *International Journal of Fracture* **60**, 169–177.

Parks, D.M. (1974). A stiffness derivative finite element technique for determination of crack tip stress intensity factors. *International Journal of Fracture* **10**, 487–501.

Qian, Z.Q. and Akisanya, A.R. (1997a). An investigation of the stress singularity near the free edge of scarf joints. Accepted for publication in *European Journal of Mechanics A/Solids*.

Qian, Z.Q. and Akisanya, A.R. (1997b). Analysis of free-edge stress and displacement fields in scarf joints subjected to a uniform change in temperature. Accepted for publication in *Fatigue and Fracture of Engineering Materials and Structures.*

Qian, Z.Q. and Akisanya, A.R. (1998). An experimental investigation of failure initiation in bonded joints. Accepted for publication in *Acta Metallurgica.*

Reedy Jr., E.D. (1990). Intensity of the stress singularity at the interface-corner between a bonded elastic and rigid layer. *Engineering Fracture Mechanics* **36**, 575–583.

Reedy Jr., E.D. (1993). Asymptotic interface-corner solutions for butt tensile joints. *International Journal of Solids and Structures* **30**, 767–777.

Reedy Jr., E.D. and Guess T.R. (1993). Comparison of butt tensile strength data with interface corner stress intensity factor prediction. *International Journal of Solids and Structures* **30**, 2929–2936.

Sinclair, G.B., Okajima, M. and Griffin, J.H. (1984). Path independent integral for computing stress intensity factors at sharp notches in elastic strips. *International Journal for Numerical Methods in Engineering* **20**, 999–1008.

Sokolnikoff, I.S. (1956). *Mathematical Theory of Elasticity* (2nd edn), McGraw Hill, New York.

Stern, M., Becker, E.D. and Dunham, R.S. (1976). A contour integral computation of mixed mode stress intensity factors. *International Journal of Fracture* **12**, 359–368.

Suga, T., Elssner, G. and Schmander, S. (1988). Composite parameters and mechanical compatibility. *Journal of Composite Materials* **22**, 917–935.

Weibull, W. (1939). Phenomenon of rupture in solids. *Ingenioersvetenskaps Akad. Handl.* **153**, 1–55.